

Thermal hysteresis in scattering by vanadium-dioxide spheres

Akhlesh Lakhtakia^{1,*}, Tom G. Mackay^{1,2}, and Waleed I. Waseer^{1,3}

¹ The Pennsylvania State University, Department of Engineering Science and Mechanics, University Park, Pennsylvania 16802, United States of America

² University of Edinburgh, School of Mathematics and Maxwell Institute for Mathematical Sciences, Edinburgh EH9 3FD, Scotland, UK

³ COMSATS University Islamabad, Department of Electrical and Computer Engineering, Islamabad, Pakistan

*Corresponding author: akhlesh@psu.edu

Abstract

Vanadium dioxide (VO_2) transforms from purely monoclinic to purely tetragonal on being heated from 58 °C to 72 °C, the transformation being reversible but hysteretic. Electromagnetically, VO_2 transforms from a dissipative dielectric to another dissipative dielectric if the free-space wavelength $\lambda_0 < 1100$ nm, but from a dissipative dielectric to a plasmonic metal (or *vice versa*) if $\lambda_0 > 1100$ nm. Calculating the extinction, total scattering, absorption, radiation-pressure, back-scattering, and forward-scattering efficiencies of a VO_2 sphere, we found clear signatures of thermal hysteresis in (i) the forward-scattering, back-scattering, and absorption efficiencies for $\lambda_0 < 1100$ nm, and (ii) the forward-scattering, back-scattering, total scattering, and absorption efficiencies for $\lambda_0 > 1100$ nm. Vacuum and null-permittivity quasistates occur between 58 °C and 72 °C, when tetragonal VO_2 is a plasmonic metal, once each on the heating branch and once each on the cooling branch of thermal hysteresis. But none of the six efficiencies show significant differences between the two quasistates.

1 Introduction

Vanadium dioxide (VO_2) is monoclinic at any temperature $T \lesssim 58$ °C but tetragonal for $T \gtrsim 72$ °C. The crystal structure changes as the temperature is raised from below 58 °C to above 72 °C [1], a mixture of crystals of both types existing in the intermediate thermal regime [2]. During the transformation, the vanadium–vanadium atomic pairs located periodically in the monoclinic crystal separate into single atoms located periodically in the tetragonal crystal [3], the mass density increases by 1.79%, and the electrical conductivity increases by at least three orders of magnitude [1, 4]. Not only is the transformation thermally reversible, its electromagnetic consequences are clearly evident in the sub-megahertz [5], megahertz [6], gigahertz [4, 7], far-infrared [8, 9], mid-infrared [2], near-infrared [10, 11], and visible [10, 12] spectral regimes. Therefore, this material is attractive for a variety of switching applications [13–17].

Monoclinic VO_2 is a dissipative insulator, i.e., both the real and the imaginary parts of the relative permittivity $\epsilon_{\text{vo}}^{\text{mono}}$ are positive, with $\text{Re}\{\epsilon_{\text{vo}}^{\text{mono}}\}$ significantly larger than $\text{Im}\{\epsilon_{\text{vo}}^{\text{mono}}\}$ in the visible and sub-visible spectral regimes [2–12]. However, tetragonal VO_2 is a dissipative insulator only when the free-space wavelength $\lambda_0 \lesssim 1100$ nm [12], with $\text{Re}\{\epsilon_{\text{vo}}^{\text{tetra}}\} > 0$ and $\text{Im}\{\epsilon_{\text{vo}}^{\text{tetra}}\} > 0$. But $\text{Re}\{\epsilon_{\text{vo}}^{\text{tetra}}\} < 0$ and $\text{Im}\{\epsilon_{\text{vo}}^{\text{tetra}}\} > 0$ for $\lambda_0 \gtrsim 1100$ nm, so that tetragonal VO_2 then functions as a plasmonic metal. The complete insulator-to-metal transformation (IMT) on heating by 14 °C and the complete metal-to-insulator transformation (MIT) on cooling by 14 °C, at reasonably low temperatures in the neighborhood of 65 °C, are responsible for the attraction of VO_2 for switching applications for $\lambda_0 \gtrsim 1100$ nm [13–17]. These applications are premised on two unambiguous states: the ON state in which VO_2 is purely monoclinic/tetragonal and the OFF state in which VO_2 is purely tetragonal/monoclinic.

Although reversible, the thermal transformation is hysteretic. In other words, the properties of VO_2 in the intermediate thermal regime (58 °C to 72 °C) depend on whether the material is being heated/cooled from having only monoclinic/tetragonal crystals to having only tetragonal/monoclinic ones. The electromagnetic

consequences of thermal hysteresis remain obscure, although the relative permittivity $\varepsilon_{\text{vo}}(\lambda_0, T)$ has been investigated on both the heating and the cooling branches by a few researchers [2, 10, 18].

Scattering by an isotropic dielectric sphere is a basic electromagnetic boundary-value problem [19], with its solution traceable to Lorenz [20, 21], Mie [22], and Debye [23]. Since $\varepsilon_{\text{vo}}(\lambda_0, T)$ in the intermediate thermal regime is bounded by $\varepsilon_{\text{vo}}^{\text{mono}}(\lambda_0)$ and $\varepsilon_{\text{vo}}^{\text{tetra}}(\lambda_0)$ [2, 10, 18], and $\varepsilon_{\text{vo}}^{\text{mono}}(\lambda_0)$ differs from $\varepsilon_{\text{vo}}^{\text{tetra}}(\lambda_0)$, the scattering characteristics of a VO₂ sphere of radius a at any specific value of λ_0 will depend not only on the ratio $\bar{a} = a/\lambda_0$ but also on T . If these characteristics on the heating branch are sufficiently different from those on the cooling branch, they could be useful in determining not only the ambient temperature $T \in [58^\circ\text{C}, 72^\circ\text{C}]$ but also whether the surroundings of a VO₂ sphere are being heated or cooled in the intermediate thermal regime.

That idea motivated this research. Standard expressions devolving from the Lorenz–Mie theory for plane-wave scattering by an isotropic dielectric sphere [24] were used for the extinction, total scattering, absorption, radiation-pressure, back-scattering, and forward-scattering efficiencies of a VO₂ sphere. These quantities were computed as functions of temperature in the intermediate thermal regime and the manifestations of thermal hysteresis in electromagnetic scattering were identified.

2 Theoretical expressions

Suppose that a plane wave propagating in a fixed direction illuminates the sphere $r \leq a$. Then,

$$Q_{\text{ext}} = \frac{1}{2\pi^2 \bar{a}^2} \text{Re} \left\{ \sum_{n=1}^{\infty} [(2n+1)(a_n + b_n)] \right\} \quad (1)$$

is the extinction efficiency,

$$Q_{\text{sca}} = \frac{1}{2\pi^2 \bar{a}^2} \sum_{n=1}^{\infty} [(2n+1)(|a_n|^2 + |b_n|^2)] \quad (2)$$

is the total scattering efficiency,

$$Q_{\text{abs}} = Q_{\text{ext}} - Q_{\text{sca}} \quad (3)$$

is the absorption efficiency,

$$Q_{\text{pr}} = Q_{\text{ext}} - \frac{1}{\pi^2 \bar{a}^2} \text{Re} \left\{ \sum_{n=1}^{\infty} \left[\frac{n(n+2)}{n+1} (a_n^* a_{n+1} + b_n^* b_{n+1}) + \frac{2n+1}{n(n+1)} a_n^* b_n \right] \right\} \quad (4)$$

is the radiation-pressure efficiency with the asterisk denoting the complex conjugate,

$$Q_{\text{b}} = \frac{1}{4\pi^2 \bar{a}^2} \left| \sum_{n=1}^{\infty} [(-)^n (2n+1)(a_n - b_n)] \right|^2 \quad (5)$$

is the back-scattering efficiency, and

$$Q_{\text{f}} = \frac{1}{4\pi^2 \bar{a}^2} \left| \sum_{n=1}^{\infty} [(2n+1)(a_n + b_n)] \right|^2 \quad (6)$$

is the forward-scattering efficiency [24–26]. The coefficients

$$\left. \begin{aligned} a_n &= \frac{\varepsilon_{\text{vo}} j_n(2\pi \bar{a} n_{\text{vo}}) \psi_n^{(1)}(2\pi \bar{a}) - j_n(2\pi \bar{a}) \psi_n^{(1)}(2\pi \bar{a} n_{\text{vo}})}{\varepsilon_{\text{vo}} j_n(2\pi \bar{a} n_{\text{vo}}) \psi_n^{(3)}(2\pi \bar{a}) - h_n^{(1)}(2\pi \bar{a}) \psi_n^{(1)}(2\pi \bar{a} n_{\text{vo}})} \\ b_n &= \frac{j_n(2\pi \bar{a} n_{\text{vo}}) \psi_n^{(1)}(2\pi \bar{a}) - j_n(2\pi \bar{a}) \psi_n^{(1)}(2\pi \bar{a} n_{\text{vo}})}{j_n(2\pi \bar{a} n_{\text{vo}}) \psi_n^{(3)}(2\pi \bar{a}) - h_n^{(1)}(2\pi \bar{a}) \psi_n^{(1)}(2\pi \bar{a} n_{\text{vo}})} \end{aligned} \right\}, \quad (7)$$

emerge from the solution of a boundary-value problem [24], with

$$\left. \begin{aligned} n_{\text{VO}} &= \sqrt{\epsilon_{\text{VO}}} \\ \psi_n^{(1)}(u) &= \frac{d}{du} [u j_n(u)] \\ \psi_n^{(3)}(u) &= \frac{d}{du} [u h_n^{(1)}(u)] \end{aligned} \right\}, \quad (8)$$

where $j_n(u)$ is the spherical Bessel function of order n and argument u and $h_n^{(1)}(u)$ is the spherical Hankel function of the first kind, order n , and argument u . An $\exp(-i\omega t)$ dependence on time t is implicit, with $i = \sqrt{-1}$ and ω denoting the angular frequency.

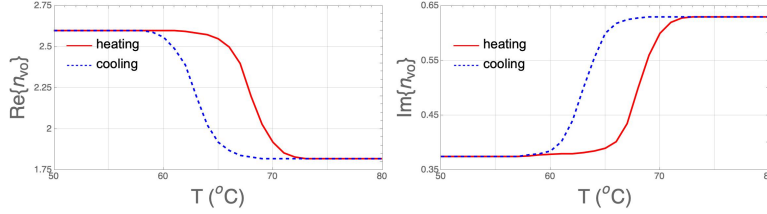


Figure 1: $\text{Re}\{n_{\text{VO}}\}$ and $\text{Im}\{n_{\text{VO}}\}$ as functions of T for $\lambda_0 = 800$ nm [10].

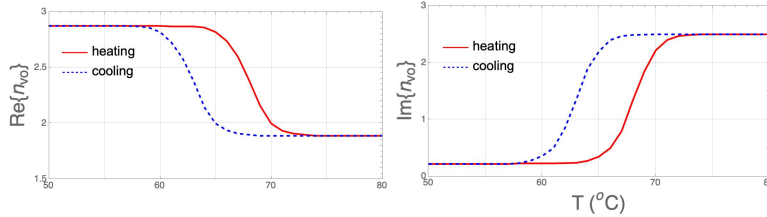


Figure 2: Same as Fig. 1 except for $\lambda_0 = 1550$ nm [10].

3 Numerical Results and Discussion

Figures 1 and 2 present the real and imaginary parts of n_{VO} as functions of T for $\lambda_0 = 800$ nm and $\lambda_0 = 1550$ nm, respectively [10]. Since $\text{Re}\{n_{\text{VO}}^{\text{mono}}\} \simeq 7 \text{Im}\{n_{\text{VO}}^{\text{mono}}\}$ for $\lambda_0 = 800$ nm and $\text{Re}\{n_{\text{VO}}^{\text{mono}}\} \simeq 13 \text{Im}\{n_{\text{VO}}^{\text{mono}}\}$ for $\lambda_0 = 1550$ nm, monoclinic VO_2 is a moderately dissipative insulator for both wavelengths. However, $\text{Re}\{n_{\text{VO}}^{\text{tetra}}\} \simeq 3 \text{Im}\{n_{\text{VO}}^{\text{tetra}}\}$ for $\lambda_0 = 800$ nm but $\text{Re}\{n_{\text{VO}}^{\text{tetra}}\} \simeq 0.75 \text{Im}\{n_{\text{VO}}^{\text{tetra}}\}$ for $\lambda_0 = 1550$ nm. Accordingly, tetragonal VO_2 is

- (i) a more dissipative insulator than monoclinic VO_2 for $\lambda_0 = 800$ nm, but
- (ii) a plasmonic metal for $\lambda_0 = 1550$ nm.

Thus,

- (i) both heating and cooling engender an insulator-to-insulator transformation (IIT) for $\lambda_0 = 800$ nm because $\text{Re}\{\epsilon_{\text{VO}}^{\text{mono}}\} > 0$ and $\text{Re}\{\epsilon_{\text{VO}}^{\text{tetra}}\} > 0$,

but

- (ii) heating gives rise to the IMT whereas cooling creates the MIT for $\lambda_0 = 1550$ nm because $\text{Re}\{\epsilon_{\text{VO}}^{\text{mono}}\} > 0$ and $\text{Re}\{\epsilon_{\text{VO}}^{\text{tetra}}\} < 0$.

Switching applications of VO_2 exploit the IMT and MIT [13–17] but ignore the IIT and avoid the intermediate thermal regime.

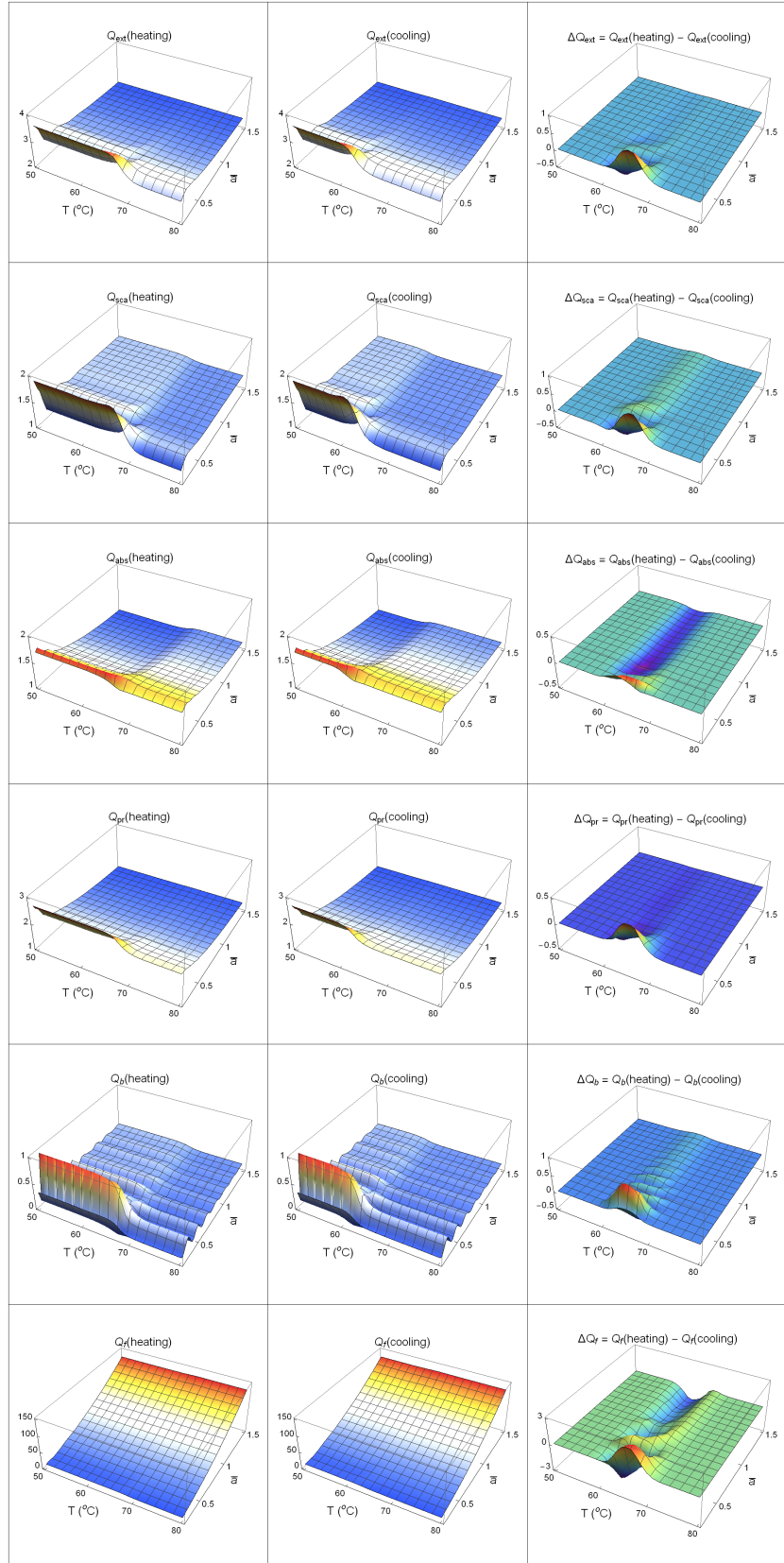


Figure 3: Q_{ext} , Q_{sca} , Q_{abs} , Q_{pr} , Q_{b} , and Q_{f} as functions of T and \bar{a} for $\lambda_0 = 800$ nm.

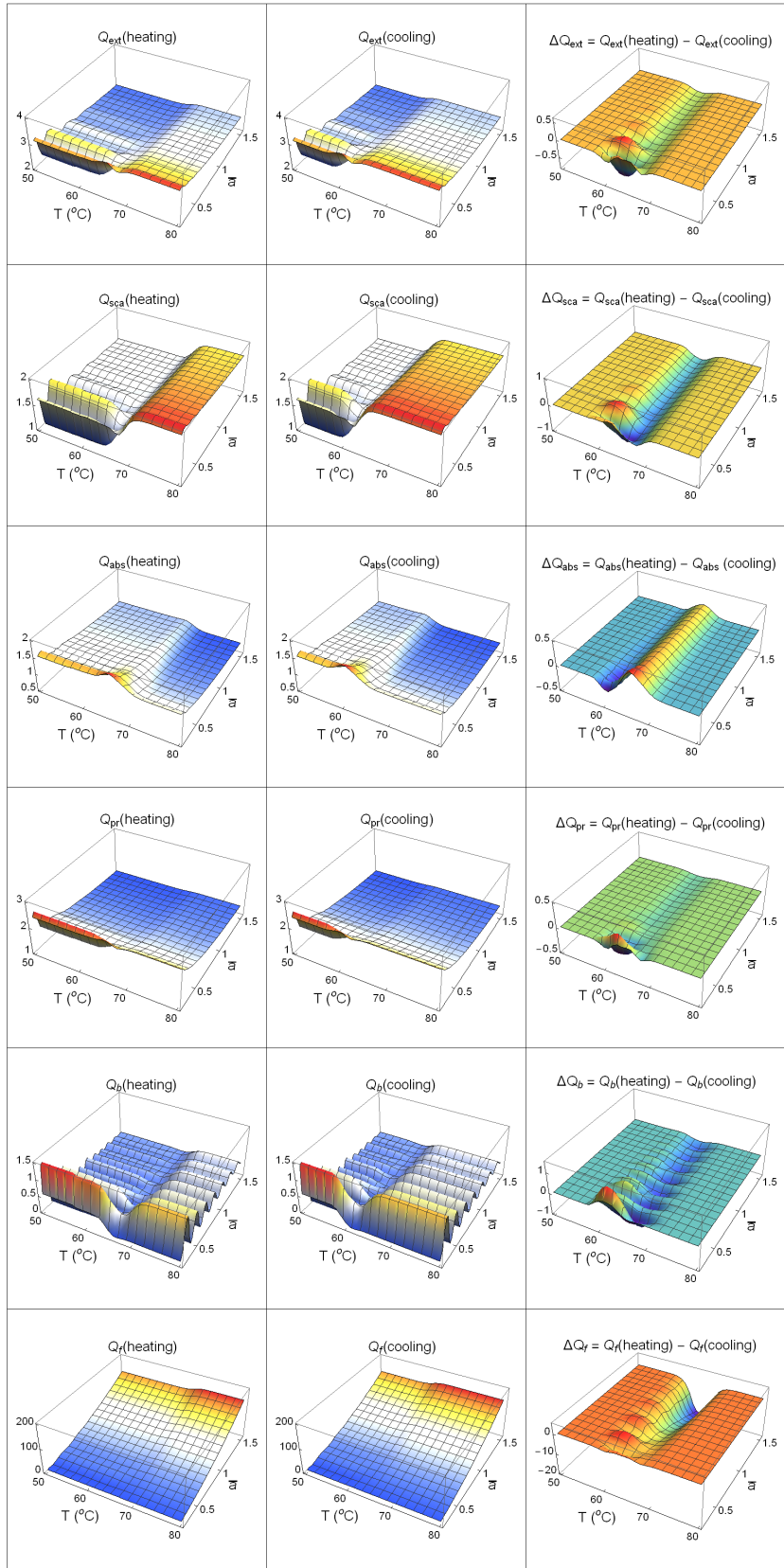


Figure 4: Same as Fig. 3 except for $\lambda_0 = 1550$ nm.

3.1 IIT/IIT ($\lambda_0 < 1100$ nm)

Both heating and cooling engender a reversible IIT for $\lambda_0 = 800$ nm, as is clear from Fig. 1. Figure 3 provides graphs of Q_{ext} , Q_{sca} , Q_{abs} , Q_{pr} , Q_{b} , and Q_{f} as functions of T and \bar{a} on both the heating and the cooling branches. The first four efficiencies in that list of six may be considered as *directionally averaged* metrics of scattering, whereas Q_{b} refers to the back-scattering direction and Q_{f} to the forward-scattering direction. Furthermore, the difference

$$\begin{aligned} \Delta Q_{\ell} &= Q_{\ell}(\text{heating}) - Q_{\ell}(\text{cooling}), \\ \ell &\in \{\text{ext, sca, abs, pr, b, f}\}, \end{aligned} \quad (9)$$

of each of the six efficiencies on the heating branch relative to its value on the cooling branch is also plotted with respect to T and \bar{a} in Fig. 3; obviously, this difference does not exist for $T \lesssim 58$ °C and $T \gtrsim 72$ °C.

All six efficiencies in Fig. 3 are different for purely monoclinic VO₂ (i.e., $T \lesssim 58$ °C) and purely tetragonal VO₂ (i.e., $T \gtrsim 72$ °C). Unsurprisingly therefore, significant dependences on temperature exist in the intermediate thermal regime on both the heating and cooling branches.

The graphs of Q_{ext} and ΔQ_{ext} indicate that the effect of thermal hysteresis on plane-wave extinction is much more pronounced when the radius of the VO₂ sphere is less than half the free-space wavelength, with ΔQ_{ext} being of the highest magnitude somewhere in the middle third of the intermediate thermal regime. As \bar{a} increases from 0.5, the effect of thermal hysteresis diminishes rapidly and is barely noticeable when $\bar{a} = 1.5$. This may be related to the fact that $Q_{\text{ext}} \rightarrow 2$ as $\bar{a} \rightarrow \infty$, regardless of the composition of the sphere [27, 28].

The effects of thermal hysteresis on Q_{sca} and Q_{abs} are much more pronounced when $\bar{a} \lesssim 0.5$. Both ΔQ_{sca} and ΔQ_{abs} are also of the highest magnitude somewhere in the middle third of the intermediate thermal regime. Their magnitudes diminish as \bar{a} increases beyond about 0.5, with ΔQ_{sca} and ΔQ_{abs} roughly equal in magnitude but opposite in sign, which is not surprising since $\Delta Q_{\text{ext}} = \Delta Q_{\text{sca}} + \Delta Q_{\text{abs}}$.

The graphs of Q_{pr} and ΔQ_{pr} are similar to those of Q_{ext} and ΔQ_{ext} , respectively. Hence, the effect of thermal hysteresis on radiation-pressure efficiency is much more pronounced for $\bar{a} \lesssim 0.5$ than for $\bar{a} \gtrsim 0.5$. The effect of the IIT is barely noticeable for any $\bar{a} \gtrsim 1$, i.e., Q_{pr} depends very weakly on T if VO₂ is purely monoclinic or purely tetragonal, or if it comprises crystals of both types in any proportion.

The back-scattering efficiency is an undulating function of \bar{a} at any $T \in [50$ °C, 80 °C], the undulations diminishing in magnitude as \bar{a} increases beyond 0.5. In general, Q_{b} is higher for purely monoclinic VO₂ than for purely tetragonal VO₂. The graph of ΔQ_{b} indicates that thermal hysteresis is most pronounced at $\bar{a} \sim 0.35$.

In contrast to Q_{b} , Q_{f} increases monotonically with $\bar{a} \in [0.25, 1.5]$ in Fig. 3 for any $T \in [50$ °C, 80 °C]. The difference ΔQ_{f} can be negative or positive as T changes in the intermediate thermal regime for $\bar{a} \lesssim 1$. However, as \bar{a} increases beyond unity, ΔQ_{f} becomes more negative.

The overall conclusions from Fig. 3 are as follows:

- Q_{ext} , Q_{sca} , Q_{abs} , Q_{pr} , and Q_{b} are higher for $T \lesssim 58$ °C (purely monoclinic) than for $T \gtrsim 72$ °C (purely tetragonal), when the sphere is small ($\bar{a} \lesssim 0.5$).
- Q_{ext} , Q_{sca} , Q_{abs} , Q_{pr} , and Q_{b} are marginally different for $T \lesssim 58$ °C (purely monoclinic) from their values for $T \gtrsim 72$ °C (purely tetragonal), when the sphere is large ($\bar{a} \gtrsim 0.5$).
- All six efficiencies are affected by thermal hysteresis most when the sphere is small ($\bar{a} \lesssim 0.5$).
- Q_{ext} and Q_{pr} are affected very little by thermal hysteresis when the sphere is large ($\bar{a} \gtrsim 0.5$).
- Q_{sca} , Q_{abs} , Q_{b} , and Q_{f} are affected steadily by thermal hysteresis as \bar{a} increases beyond unity.

3.2 IMT/MIT ($\lambda_0 > 1100$ nm)

When the free-space wavelength increases beyond 1100 nm, tetragonal VO₂ becomes a plasmonic metal whereas monoclinic VO₂ remains a dissipative insulator. The IMT/MIT is therefore very different from the IIT, as even a casual comparison of Figs. 3 (for $\lambda_0 = 800$ nm) and 4 (for $\lambda_0 = 1550$ nm) shows. Of course, every one of the six efficiencies in Fig. 4 is different for purely monoclinic VO₂ than for purely tetragonal VO₂, and there are significant dependences on temperature in the intermediate thermal regime on both the heating and cooling branches.

The graph of Q_{ext} in Fig. 4 shows that the extinction is more when VO₂ is a metal (tetragonal) rather than a dissipative dielectric (monoclinic), which is also in accord with Fig. 3. Furthermore, the graphs of Q_{ext} and ΔQ_{ext} in Fig. 4 indicate that the effect of thermal hysteresis on plane-wave extinction is somewhat more pronounced for $\bar{a} \lesssim 0.5$ than for $\bar{a} \gtrsim 0.5$. Whereas ΔQ_{ext} can assume both negative and positive values for $\bar{a} \lesssim 0.5$ in the intermediate thermal regime, it is predominantly negative for $\bar{a} \gtrsim 0.5$ in the same regime. Certainly, as $\bar{a} \rightarrow \infty$ Q_{ext} must go to 2 [27,28], but at a considerably slower rate with the increase in \bar{a} than in Fig. 3.

Also, whereas ΔQ_{sca} has a bump and ΔQ_{abs} has a trough that roughly compensate each other for Q_{ext} to be barely affected by thermal hysteresis for $\bar{a} \gtrsim 0.5$ in Fig. 3, ΔQ_{sca} has a trough and ΔQ_{abs} has a bump that do not compensate each other so that Q_{ext} is affected by thermal hysteresis for $\bar{a} \gtrsim 0.5$ in Fig. 4.

Unlike in Fig. 3, the graphs of Q_{pr} in Fig. 4 are qualitatively different from those of Q_{ext} . The signature of thermal hysteresis for $\bar{a} \gtrsim 0.5$ is somewhat more marked when IMT/MIT occur than when IIT occurs.

The back-scattering efficiency is an undulating function of \bar{a} at any $T \in [50^\circ\text{C}, 80^\circ\text{C}]$, the undulations diminishing in magnitude as \bar{a} increases beyond 0.5. In general, Q_{b} is lower for purely monoclinic VO₂ than for purely tetragonal VO₂, contrary to Fig. 3. The graph of ΔQ_{b} indicates that thermal hysteresis is most pronounced at $\bar{a} \sim 0.3$.

The forward-scattering efficiency increases monotonically with $\bar{a} \in [0.25, 1.5]$ in Fig. 4 for any $T \in [50^\circ\text{C}, 80^\circ\text{C}]$, in contrast to Q_{b} . The same tendency is evident in Fig. 3. However, Q_{f} is higher when tetragonal VO₂ is a plasmonic metal (Fig. 4) than when it is a dissipative dielectric (Fig. 3). Also, ΔQ_{f} is more noticeably negative in the intermediate thermal regime as \bar{a} increases beyond unity when the IMT/MIT (Fig. 4) occur than when the IIT occurs (Fig. 3).

The overall conclusions from Fig. 4 are as follows:

- Q_{ext} , Q_{sca} , Q_{b} , and Q_{f} are noticeably lower for $T \lesssim 58^\circ\text{C}$ (purely monoclinic) than for $T \gtrsim 72^\circ\text{C}$ (purely tetragonal), when the sphere is small ($\bar{a} \lesssim 0.5$). Q_{sca} shows the opposite trend, whereas Q_{pr} is about the same for both $T \lesssim 58^\circ\text{C}$ and $T \gtrsim 72^\circ\text{C}$.
- All six efficiencies are affected by thermal hysteresis, regardless of the sphere radius.
- Q_{ext} , Q_{sca} , Q_{abs} , Q_{pr} , and Q_{b} are affected steadily by thermal hysteresis as \bar{a} increases beyond unity.
- Q_{ext} , Q_{sca} , Q_{abs} , Q_{b} , and Q_{f} are affected more in the intermediate thermal regime when tetragonal VO₂ is a plasmonic metal (Fig. 4) than a dissipative dielectric (Fig. 3).

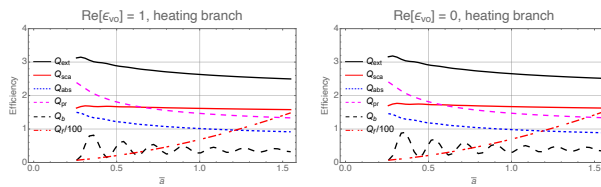


Figure 5: Q_{ext} , Q_{sca} , Q_{abs} , Q_{pr} , Q_{b} , and Q_{f} as functions of \bar{a} on the heating branch when $\lambda_0 = 1550$ nm. Left: $T = 69.11^\circ\text{C}$ ($\text{Re}\{\epsilon_{\text{vo}}\} = 1 + 8.09i$). Right: $T = 69.57^\circ\text{C}$ ($\text{Re}\{\epsilon_{\text{vo}}\} = 8.50i$).

3.3 Vacuum and null-permittivity quasistates

The IMT/MIT also serves as a route to two electromagnetic quasistates of matter. The first is the *vacuum quasistate* [29]: $\text{Re}\{\varepsilon_{\text{vo}}\} = 1$. The second is the *null-permittivity quasistate* [30]: $\text{Re}\{\varepsilon_{\text{vo}}\} = 0$. Both quasistates are exhibited by many materials that undergo temperature-mediated IMT/MIT, a very good example being indium antimonide (InSb) [31,32]. However, the IMT/MIT exhibited by InSb is not hysteretic, in contrast to VO_2 .

For $\lambda_0 = 1550$ nm, we estimated from Fig. 2 that

- $\varepsilon_{\text{vo}} = 1 + 8.09i$ at $T = 69.11$ °C and
- $\varepsilon_{\text{vo}} = 8.50i$ at $T = 69.57$ °C

on the heating branch, whereas

- $\varepsilon_{\text{vo}} = 1 + 8.13i$ at $T = 64.01$ °C and
- $\varepsilon_{\text{vo}} = 8.50i$ at $T = 64.55$ °C

on the cooling branch. Figure 5 shows all six efficiencies as functions of \bar{a} when VO_2 is in the vacuum and null-permittivity quasistates on the heating branch. Since the values of $\text{Im}\{\varepsilon_{\text{vo}}\}$ are roughly the same in both quasistates and considerably exceed unity, there is practically no distinction in the efficiencies for the two quasistates. As similar findings apply on the cooling branch, there is no need to present the corresponding graphs of the six efficiencies.

4 Concluding Remarks

As temperature changes from about 58 °C to 72 °C, the crystal structure of VO_2 transforms from purely monoclinic to purely tetragonal, the transformation being reversible but hysteretic. We have studied the response characteristics of a VO_2 sphere to planewave illumination to examine the effects of thermal hysteresis on the extinction, total scattering, absorption, radiation-pressure, back-scattering, and forward-scattering efficiencies.

Whereas monoclinic VO_2 is a dissipative dielectric, tetragonal VO_2 is a plasmonic metal for $\lambda_0 > 1100$ nm but a dissipative dielectric for $\lambda_0 < 1100$ nm. Thus, two distinct types of reversible but hysteretic transformations are possible. Clear signatures of thermal hysteresis in the insulator-to-insulator transformation are to be found in Q_f , Q_{abs} , and Q_b (in that order, in our opinion). Clear signatures of thermal hysteresis in the insulator/metal-to-metal/insulator transformation are to be found in Q_f , Q_{abs} , Q_{sca} , and Q_b (in that order). The contrast between the two dissipative dielectric forms of VO_2 ($\lambda_0 < 1100$ nm) being less pronounced than the contrast between the dissipative dielectric and the metallic forms of VO_2 ($\lambda_0 > 1100$ nm), the IMT/MIT has clearer signatures of thermal hysteresis than the IIT.

Thermal hysteresis is responsible for the double occurrences of the vacuum and null-permittivity quasistates in the intermediate thermal regime when tetragonal VO_2 is a plasmonic metal. However, none of the six efficiencies show significant differences between the two quasistates of VO_2 .

The electromagnetic consequences of thermal hysteresis exhibited by VO_2 may depend on the rate of heating or cooling, but that dependence has turned out to be difficult to characterize [33]. Photoexcitation by a free-electron laser has been shown to effect the monoclinic-to-tetragonal transformation within 150 fs [34], but not the reverse transformation—which does require cooling.

Acknowledgments. AL thanks the Charles Godfrey Binder Endowment at Penn State for ongoing support of his research efforts. WIW thanks the Higher Education Commission of Pakistan for an IRSIP Scholarship that enabled him to spend six months at The Pennsylvania State University.

References

- [1] F. J. Morin, “Oxides which show a metal-to-insulator transition at the Neel (*sic*) temperature,” *Phys. Rev. Lett.* **3**, 34–36 (1959).
- [2] H. S. Choi, J. S. Ahn, J. H. Jung, T. W. Noh, and D. H. Kim, “Mid-infrared properties of a VO₂ film near the metal-insulator transition,” *Phys. Rev. B* **54**, 4621–4628 (1996).
- [3] T. Hörlin, T. Niklewski and M. Nygren, “Electrical and magnetic properties of V_{1-x}W_xO₂, 0 ≤ x ≤ 0.060,” *Mater. Res. Bull.* **7**, 1515–1524 (1972).
- [4] A. Crunteanu, J. Givernaud, J. Leroy, D. Mardivirin, C. Champeaux, J.-C. Orlianges, A. Catherinot, and P. Blondy, “Voltage- and current-activated metal–insulator transition in VO₂-based electrical switches: a lifetime operation analysis,” *Sci. Technol. Adv. Mater.* **11**, 065002 (2010).
- [5] A. Mansingh, R. Singh, and M. Sayer, “Dielectric behavior of vanadium oxide,” *Phys. Stat. Sol. A* **49**, 773–779 (1978).
- [6] Z. Yang, C. Ko, V. Balakrishnan, G. Gopalakrishnan, and S. Ramanathan, “Dielectric and carrier transport properties of vanadium dioxide thin films across the phase transition utilizing gated capacitor devices,” *Phys. Rev. B* **82**, 205101 (2010).
- [7] N. Émond, A. Hendaoui, S. Delprat, M. Chaker, and K. Ye, “Theoretical and experimental investigation of thermo-tunable metal–insulator–vanadium dioxide coplanar waveguide structure,” *IEEE Trans. Microw. Theory Tech.* **65**, 1443–1455 (2017).
- [8] M. Gao, X. Wang, S. Luo, Q. Lu, S.-N. Luo, C. Lu, S. Chen, F. Long, and Y. Lin, “Terahertz transmission properties of vanadium dioxide films deposited on gold grating structure with different periods,” *Mater. Res. Express* **7**, 056404 (2020).
- [9] E. P. J. Parrott, C. Han, F. Yan, G. Humbert, A. Bessaudou, A. Crunteanu, and E. Pickwell-MacPherson, “Vanadium dioxide devices for terahertz wave modulation: a study of wire grid structures,” *Nanotechnology* **27**, 205206 (2016).
- [10] P. Cormier, T. V. Son, J. Thibodeau, A. Doucet, V.-V. Truong, A. Haché, “Vanadium dioxide as a material to control light polarization in the visible and near infrared,” *Opt. Commun.* **382**, 80–85 (2017).
- [11] D. J. Skelton, K. R. Coffey, and G. D. Boreman, “Experimental demonstration of tunable phase in a thermochromic infrared-reflectarray metamaterial,” *Opt. Express* **18**, 1330–1335 (2010).
- [12] P. Kepič, F. Ligmajer, M. Hrtoň, H. Ren, L. de S. Menezes, S. A. Maier, and T. Šikola, “Optically tunable Mie resonance VO₂ nanoantennas for metasurfaces in the visible,” *ACS Photonics* **8**, 1048–1057 (2021).
- [13] F. Dumas-Bouchiat, C. Champeaux, A. Catherinot, A. Crunteanu, and P. Blondy, “rf-microwave switches based on reversible semiconductor-metal transition of VO₂ thin films synthesized by pulsed-laser deposition,” *Appl. Phys. Lett.* **91**, 223505 (2007).
- [14] D. Wang, L. Zhang, Y. Gu, M. Q. Mehmood, Y. Gong, A. Srivastava, L. Jian, T. Venkatesan, C.-W. Qiu, and M. Hong, “Switchable ultrathin quarter-wave plate in terahertz using active phase-change metasurface,” *Sci. Rep.* **5**, 15020 (2015).
- [15] M. R. M. Hashemi, S.-H. Yang, T. Wang, N. Sepúlveda, and M. Jarrahi, “Electronically-controlled beam- steering through vanadium dioxide metasurfaces,” *Sci. Rep.* **6**, 35439 (2016).

- [16] A. Tripathi, J. John, S. Kruk, Z. Zhang, H. S. Nguyen, L. Berguiga, P. Rojo Romeo, R. Orobtcouk, S. Ramanathan, Y. Kivshar, and S. Cuff, “Tunable Mie-resonant dielectric metasurfaces based on VO₂ phase-transition materials,” *ACS Photonics* **8**, 1206–1213 (2021).
- [17] A. E. Serebryannikov, A. Lakhtakia, G. A. E. Vandenbosch, and E. Ozbay, “Transmissive terahertz metasurfaces with vanadium dioxide split-rings and grids for switchable asymmetric polarization manipulation,” *Sci. Rep.* **12**, 3518 (2022).
- [18] S. Taylor, L. Long, and L. Wang, “Fabrication and characterization of furnace oxidized vanadium dioxide thin films,” *Thin Solid Films* **682**, 29–36 (2019).
- [19] N. A. Logan, “Survey of some early studies of the scattering of plane waves by a sphere,” *Proc. IEEE* **53**, 773–785 (1965).
- [20] L. Lorenz, “Lysbevægelsen i og uden for en af plane Lysbølger belyst Kugle,” *K. Dan. Vidensk. Selsk. Skr., Naturvidensk. Math. Afd.* **6**, 1–62 (1890).
- [21] L. Lorenz, “Sur la lumière réfléchiée et réfractée par une sphère transparente,” in *Oeuvres Scientifiques de L. Lorenz, Revues et annotées par H. Valentine* (Librairie Lehman & Stage, Copenhagen, Denmark, 1898), Vol. 1, pp. 403–502. This French translation of Ref. 20 is accompanied by 27 pages of notes.
- [22] G. Mie, “Beiträge zur Optik trüber Medien, speziell kolloidaler Metallösungen,” *Ann. Phys. (Leipzig) Ser. 4* **25**, 377–445 (1908).
- [23] P. Debye, “Der Lichtdruck auf Kugeln von beliebigem Material,” *Ann. Phys. (Leipzig) Ser. 4* **30**, 57–136 (1909).
- [24] C. F. Bohren and D. R. Huffman, *Absorption and Scattering of Light by Small Particles* (Wiley, New York, NY, USA, 1983).
- [25] A. Lakhtakia, “Scattering by a nihility sphere,” *Microw. Opt. Technol. Lett.* **48**, 895–896 (2006).
- [26] A. Lakhtakia, “Radiation pressure efficiencies of spheres made of isotropic, achiral, passive, homogeneous, negative-phase-velocity materials,” *Electromagnetics* **28**, 346–353 (2008).
- [27] L. Brillouin, “The scattering cross section of spheres for electromagnetic waves,” *J. Appl. Phys.* **20**, 1110–1125 (1949).
- [28] M. J. Berg, C. M. Sorensen, and A. Chakrabarti, “A new explanation of the extinction paradox,” *J. Quant. Spectrosc. Rad. Transf.* **112**, 1170–1181 (2011).
- [29] A. E. Serebryannikov, A. Lakhtakia, M. Aalizadeh, E. Ozbay, and G. A. E. Vandenbosch, “Temperature-mediated invocation of the vacuum state for switchable ultrawide-angle and broadband deflection,” *Sci. Rep.* **8**, 15044 (2018).
- [30] X. Niu, X. Hu, S. Chu, and Q. Gong, “Epsilon-near-zero photonics: A new platform for integrated devices,” *Adv. Opt. Mater.* **6**, 1701292 (2018).
- [31] T. G. Mackay and A. Lakhtakia, “Temperature-mediated transition from Dyakonov surface waves to surface-plasmon-polariton waves,” *IEEE Photon. J.* **8**, 4802813 (2016).
- [32] H. M. Alkhoori and A. Lakhtakia, “Thermally controllable reduction of absorption and extinction of a dielectric sphere by an InSb coating,” *Optik* **260**, 168992 (2022).
- [33] A. Haché, personal communication to A. Lakhtakia and T. G. Mackay (29 April 2022).
- [34] S. Wall, S. Yang, L. Vidas, M. Chollet, J. M. Glowina, M. Kozina, T. Katayama, T. Henighan, M. Jiang, T. A. Miller, D. A. Reis, L. A. Boatner, O. Delaire, and M. Trigo, “Ultrafast disordering of vanadium dimers in photoexcited VO₂,” *Science* **362**, 572–576 (2018).